

# Observations of Plasmarons in a System of Massive Electrons

OE Dial,<sup>1\*</sup> RC Ashoori<sup>1</sup>, LN Pfeiffer<sup>2</sup> KW West<sup>2</sup>

<sup>1</sup>Massachusetts Institute of Technology, Cambridge, MA 02139

<sup>2</sup>Princeton, Princeton, NJ 08544

\*To whom correspondence should be addressed; E-mail: dial@alum.mit.edu.

**Calculations of the single particle density of states (SPDOS) of electron liquids have long predicted that there exist two distinct charged excitations: the usual quasiparticle consisting of an electron or hole screened by a correlation hole, and a “plasmaron” consisting of a hole resonantly bound to real plasmons in the Fermi sea (1, 2). Using tunneling spectroscopy to measure the SPDOS of a two-dimensional electronic system, we demonstrate the first detection of the plasmaron in a system in which electrons have mass. We monitor the evolution of the plasmaron with applied magnetic field and discover unpredicted “magnetoplasmarons” which appear in spectra as negative index Landau levels. These sharp features corresponding to long-lived quasiparticles appear at high energies where SPDOS structure is ordinarily broadened by electron-electron interactions.**

The “plasmaron” was originally proposed by Hedin and Lundquist (1, 2) to exist in three-dimensional (3D) metals. However, aside from the unusual semi-metal Bismuth (3), it has not been unambiguously observed in 3D, and some theories suggest that the 3D plasmaron

should not exist (4). In contrast, more recent theories predict a robust plasmaron in two-dimensional electronic systems (2DESs) (5–9). Indeed, the plasmaron has recently been observed in graphene, which contains a 2DES with massless electrons (10). We observe several key differences between our observation of the plasmaron in system with massive electrons and the experimental and theoretical results for graphene. Whereas in graphene the plasmaron is predicted to exist both above and below the Fermi energy (8) and exhibits a simple scaling law with electron density, we find that in a system of massive electrons the plasmaron exhibits a strong asymmetry about the Fermi energy and exhibits a non-linear and unpredicted dependence on electron density.

We perform our tunneling measurements using time domain capacitance spectroscopy (TDCS) (11–13). This technique allows the measurement of the SPDOS with precisely calibrated energy and density axes and minimal effects of heating. In TDCS, the 2DES to be studied is grown epitaxially inside of a capacitor. One plate of the capacitor, the tunnel electrode, is close enough to allow charge to tunnel to and from the 2D system. The other plate is distant enough to be electrically isolated and is used to detect the tunnel current by means of its image charge. DC voltages can be used to tune the density of the 2D system continuously, while tunnel voltages and currents can be induced by applying voltage pulses across the capacitor. In the present measurements the 2DES is a 230Å GaAs quantum well. The plates of the capacitor are 3D doped regions of GaAs with an electron density of  $1 \times 10^{18} \text{cm}^{-2}$ . The tunnel electrode is separated from the 2DES by a 130Å tunnel barrier of  $x = .324 \text{ Al}_x\text{Ga}_{1-x}\text{As}$  followed by 300Å of undoped GaAs which acts as a spacer layer to reduce scattering (14). This spacer is thin enough it is populated by electrons due to the finite Thomas-Fermi screening length. The electrically isolated electrode is separated from the 2DES by 600Å of  $x = .324 \text{ Al}_x\text{Ga}_{1-x}\text{As}$ .

Figure 1a shows a typical TDCS spectrum acquired at 100 mK with zero magnetic field. The horizontal axis is the density in the 2DES, which is controlled by the DC bias across the

device. The vertical axis is energy, with  $E=0$  corresponding to the Fermi energy. The band edge of the 2DES, corresponding to injecting a wavevector  $k = 0$  hole, is visible as a abrupt edge that begins near  $E = 0$  at zero density and moves downward in energy as the 2D system is populated (Solid arrows in figure 1b). Tunneling matrix element effects reduce the tunnel current at high energies and densities, causing the 2D band to appear as a peak rather than a step (12, 14). Because of the additional energy to create the plasmon, creating a plasmaron requires more energy than creating an ordinary hole. More energetic holes occur at more negative energies in our spectra. Thus, the plasmaron appears as a second edge below the 2D band edge in the spectrum (dashed arrows in 1b). Both edges can be emphasized by differentiating the data with respect to tunnel voltage to provide  $d^2I/dV^2$  and smoothing it by convolving with a  $\sigma = 190\mu\text{eV}$  Gaussian to remove resulting high frequency noise (figure 1d).

We identify the edges of the 2D and plasmaron band edges by the location of the peak in  $d^2I/dV^2$  (figure 1c). At densities above  $5 \times 10^{10}$ , the 2D band edge lies at  $E_{2d} = (-0.403 \pm 0.003)\text{meV} \times N_{2d}/(10^{10}\text{cm}^{-2}) + (0.2 \pm 0.01)\text{meV}$ , where  $N_{2d}$  is the electron density of the 2DES. The offset is due to our choice of the peak in the derivative of the TDOS as our band edge. For a non-interacting system,  $m^* = \pi\hbar^2/(dE_{2d}/dN_{2d})$ , allowing us to extract  $m^* = 0.060 \pm 0.001m_0$ , where the error is dominated by systematic errors in the calibration of the lever arm. This is slightly smaller than the bulk value of  $m^* = 0.063$  assumed in the energy calibration, implying a somewhat larger energy bandwidth than expected. Note this bandwidth is the energy difference between suddenly creating a hole at the bottom of the band and suddenly creating one at the Fermi energy, and it is not in general equal to the chemical potential. While the details giving rise to this larger bandwidth are complex, we note that both band-nonparabolicity (15) and interaction effects (6) are expected to increase this bandwidth slightly.

We find a good empirical fit for the location of the plasmaron edge to be  $E_{pl} = E_{2d} - (1.53 \pm 0.02\text{meV}) \times \sqrt{N_{2d}/(10^{10}\text{cm}^{-2})} - 0.2 \pm 0.01\text{meV}$ . While this density dependence has not been

predicted in the literature, we note the overall  $\sqrt{N_{2d}}$  is suggestive of the density dependence of the plasmon component of the plasmaron, with  $\hbar\omega_p(k) = \sqrt{nek/(2m\epsilon)}$ .

While detailed calculations of the plasmaron energy and lifetime exist elsewhere (1, 2, 4–7, 16), a simple “cartoon” model aids in developing intuition and in understanding how the heterostructure can modify the plasmaron structure. The plasmaron exists because, for a small range of energies and wavevectors, it is possible to create a composite excitation with wavevector  $k$  consisting of resonantly bound holes of wavevector  $k - q$  and plasmons of wavevector  $q$ . To create a plasmaron with energy  $E_{pl}(k)$ , this resonance condition is given by

$$E_{pl}(k) = \frac{\hbar^2 [k_f^2 - (k - q)^2]}{2m^*} + \hbar\omega_p(q) + E_c(q, k)$$

Here  $\hbar\omega_p(q)$  is the energy to create a plasmon of wavevector  $q$  (proportional to  $\sqrt{N_{2d}q}$  at small  $q$  (17)) and  $E_c$  is a coupling energy. If we momentarily neglect the coupling energy we can graphically solve for resonance by rearranging this as  $E_{pl}(k) - \hbar\omega_p(q) = \frac{\hbar^2 [k_f^2 - (k - q)^2]}{2m^*}$  (Figure 2A; note the energy axis is inverted to match the sign convention in our experimental data). On doing so, it becomes clear that for some values of  $E_{pl}(k)$ , a resonance occurs not for a single value of  $q$  but instead across a range of  $q$  vectors where the hole (blue) and plasmon (green) dispersion become tangent (red circles); the hole-plasmon coupling is strongest when the hole and plasmon group velocities match. This results in a strong resonance that allows the coherent screening of the injected quasiparticle by a cloud of real plasmons, creating a long-lived excitation at  $E_{pl}$ . As the momentum of the plasmaron  $k$  is increased (black line),  $E_{pl}$  must increase to keep the plasmon and hole dispersion curves tangent (dotted green line). At the same time, the relevant plasmon  $q$  vector increases. Because the coupling of the hole to the plasmon is through the Coulomb interaction, it dies away as  $1/q$ . This weakening of the hole-plasmon coupling together with a decrease in the resonant phase space destroys the plasmaron at large  $k$ . For typical densities in our device, this is predicted to occur at  $k \sim 0.15k_f$  (6). The plasmaron

dispersion curve and its range are pictured in black as the small upside-down u near the bottom of Figure 2a.

Because the plasmon dispersion curve becomes steeper as  $\sqrt{N_{2d}}$ , the plasmaron becomes more widely separated from the 2D band as the density is increased. At the same time, the relevant  $q$ -vector increases, weakening and ultimately destroying the plasmaron as the 2DES density is increased.

The plasmaron, then, is a long lived excitation that only exists at small wave-vectors and small electron densities. It is made up of resonantly coupled holes and plasmons of equal but opposite wavevectors centered about the  $k$  vector of the plasmaron. The wavevector of the plasmon and hole involved is large:  $\sim 0.66 k_f$  for a GaAs 2DES at  $N_{2d} = 1 \times 10^{11}$ . A comparison of the general form of the plasmaron dispersion from this argument to the Random Phase Approximation (RPA) spectral function  $A(k, \omega)$  (essentially the momentum resolved SPDOS) calculated as per [6] is included in Figure 2B.

In the case of injecting electrons into the quantum well, larger momenta  $k - q$  gives higher energy excitations rather than lower. When repeating the above discussion the parabolic electron dispersion is flipped with respect to the plasmon dispersion. The plasmon and electron curve then cross at a sharp angle rather than touching tangentially (Figure 2C). Accordingly, there is no broad region of resonance, and no long lived plasmaron above the Fermi energy. This is in marked contrast to the case in graphene, where no electron-hole asymmetry exists (8, 9).

At any given wave-vector the plasmaron is sharply peaked at a particular energy; however, when this spectrum is averaged across all wave-vectors, the added structure due to the plasmaron is expected to appear as a step, possibly with a peak at the low energy edge depending on the lifetime of the plasmaron. For an isolated quantum well of infinitesimal thickness, this edge is predicted to lie from two to six times the 2D Fermi energy below the 2D band edge at a density of  $1 \times 10^{11} \text{cm}^{-2}$ , depending on what approximation scheme is used in calculating the spectral

function. The plasmaron step appears much closer to the Fermi energy in our data, separated from the band edge by only roughly  $1.3 \times E_F$  at  $1 \times 10^{11} \text{cm}^{-2}$ . The SPDOS calculated using RPA (as in Ref [6]) for an isolated infinitely thin well is superimposed on measured spectra in figure 3 at a variety of densities, showing this discrepancy. However, because the energy of the plasmaron is extremely sensitive to both the plasmon dispersion and the Coulomb interaction, a number of features in our structure not present in the simplest calculations tend to considerably reduce the distance between the 2D band edge and the plasmaron. The  $230\text{\AA}$  wide square quantum well reduces the effective electron-electron interaction at short distances, and can be accounted for by the addition of a “form factor” to the Coulomb potential. Doing so moves the plasmaron edge somewhat closer to the band edge (figure 3). In addition, the nearby metallic tunnel electrode screens the Coulomb interaction at large distances and also tends to reduce the plasmon energy at large wavevector (18, 19); this can also be incorporated into the form factor. This further reduces the discrepancy as well as smoothing the plasmaron peak into more of a step. Finally, coupling to optical phonons modifies the dielectric function somewhat at energies and wavevectors relevant to the plasmaron, further reducing the plasmaron energy and completing the transformation of the plasmaron contribution to the SPDOS to a step rather than peak.

The calculated energy spectrum is still substantially different from the measured spectrum. RPA underestimates the screening of the Coulomb interaction by the correlation hole around injected quasiparticles; more accurate calculations would be expected to further reduce the energy of the plasmaron. The exquisite sensitivity of the plasmaron feature to the electron-electron interactions make it an excellent benchmark for testing approximate methods in many-body theories.

On applying a quantizing magnetic field, we find the plasmaron step breaks up into a series of faint “ghost” Landau levels below the 2D band edge (Figure 4A). We note that the 2D

density is measured independently using magnetocapacitance in this measurement, confirming that there is no offset on the density axis of this spectrum and thus confirming our identification of the  $N=0$  Landau level. On applying a quantizing magnetic field, the energy of creating a hole becomes non-dispersive, discretized by Landau quantization into flat bands separated by  $\hbar\omega_c$ . At the same time, the dispersion curve of magnetoplasmons is gapped by the cyclotron energy, is rather flat, and has one or more magneto-roton extrema at long wavelengths (20, 21). Thus, repeating the “cartoon” arguments applied to the zero-field plasmon, it seems reasonable for the band of plasmareons responsible for the plateau in our data to sharpen into one or more “ghost” Landau levels lying below  $N = 0$ , which we label “magnetoplasmarons” by analogy to magnetoplasmons. This is indeed observed (figure 4B); on varying the magnetic field while holding the bias voltage fixed (roughly fixing the density), a number of “ghost” Landau levels can be observed, with separations that scale with the cyclotron energy. In particular, at  $\nu = 4$  at 1 Tesla, two “magnetoplasmaron” peaks are visible below the  $N = 0$  Landau level with an inter-peak splitting of  $1.9 \pm 0.1$  meV, similar to the cyclotron energy  $\hbar\omega_c$  of 1.7 meV at this field. The splitting between the  $N=0$  Landau level and the first plasmareon peak is complicated by the exchange splitting of the bottom Landau level; however, taking the energy of the  $N = 0$  level to be the mean energy of the spin up and spin down peaks, the measured splitting is  $2.4 \pm 0.1$  meV, significantly larger than the cyclotron energy.

Once the magnetic field is applied, we chiefly observe magnetoplasmaron features within the band of energies occupied by the plasmareon plateau at zero field. The magnetoplasmaron peaks sharpen and move away from the  $N = 0$  Landau level as the cyclotron energy grows, but they largely vanish as they fall below the energy of the plasmareon edge at zero magnetic field. The exact mechanism of this cutoff at high magnetic fields is currently unknown. However, the polarizability of the 2DES at high magnetic field has a similar overall envelope to that at zero magnetic field (22); this may be responsible for the similar cutoff energies and densities.

Due to the accumulated expertise in fabricating nano-scale structures in GaAs, the existence of plasmarons in this system may lead to new applications and research lines. Normally high energy quasiparticles in Fermi liquids are short-lived due to decay by particle-hole creation. In contrast, plasmarons are predicted to be long-lived, creating the possibility of accurate high energy spectroscopy and barrier transmission measurements. Furthermore, the plasmaron carries charge and can in principle easily be manipulated and focused in GaAs using electrostatic gates (23, 24). Finally, the plasmon component of the plasmaron can strongly couple it to terahertz light, creating the possibility of novel electro-optical devices.

## References and Notes

1. L. Hedin, B. Lundqvist, S. Lundqvist, *Solid State Communications* **5**, 237 (1967).
2. B. I. Lundqvist, *Zeitschrift für Physik B Condensed Matter* **6**, 193 (1967).
3. R. Tediosi, N. P. Armitage, E. Giannini, D. van der Marel, *Phys. Rev. Lett.* **99**, 016406 (2007).
4. B. Bergersen, F. Kus, C. Bolmberg, *Can. J. Phys.* **51**, 102 (1973).
5. P. von Allmen, *Phys. Rev. B* **46**, 13345 (1992).
6. R. Jalabert, S. Das Sarma, *Phys. Rev. B* **39**, 5542 (1989).
7. R. Jalabert, S. Das Sarma, *Phys. Rev. B* **40**, 9723 (1989).
8. E. H. Hwang, S. Das Sarma, *Phys. Rev. B* **77**, 081412 (2008).
9. M. Polini, *et al.*, *Phys. Rev. B* **77**, 081411 (2008).
10. A. Bostwick, *et al.*, *Science* **328**, 999 (2010).



11. H. B. Chan, P. I. Glicofridis, R. C. Ashoori, M. R. Melloch, *Phys. Rev. Lett.* **79**, 2867 (1997).
12. O. E. Dial, R. C. Ashoori, L. N. Pfeiffer, K. W. West, *Nature* **448**, 176 (2007).
13. O. E. Dial, R. C. Ashoori, L. N. Pfeiffer, K. W. West, *Nature* **464**, 566 (2010).
14. J. A. Lebens, R. H. Silsbee, S. L. Wright, *Appl. Phys. Lett.* **51**, 840 (1987).
15. E. O. Kane, *Journal of Physics and Chemistry of Solids* **1**, 249 (1957).
16. C. Guillemot, F. Clérot, *Phys. Rev. B* **47**, 7227 (1993).
17. F. Stern, *Phys. Rev. Lett.* **18**, 546 (1967).
18. A. Eguluz, T. K. Lee, J. J. Quinn, K. W. Chiu, *Phys. Rev. B* **11**, 4989 (1975).
19. E. H. Hwang, S. Das Sarma, *Phys. Rev. B* **64**, 165409 (2001).
20. C. Kallin, B. I. Halperin, *Phys. Rev. B* **30**, 5655 (1984).
21. C. Kallin, B. I. Halperin, *Phys. Rev. B* **31**, 3635 (1985).
22. R. Roldán, M. O. Goerbig, J.-N. Fuchs, *Semiconductor Science and Technology* **25**, 034005 (2010).
23. J. Spector, H. Stormer, K. Baldwin, L. Pfeiffer, K. West, *Appl. Phys. Lett.* **56**, 1290 (1990).
24. U. Sivan, M. Heiblum, C. P. Umbach, H. Shtrikman, *Phys. Rev. B* **41**, 7937 (1990).
25. O.E.D. built the apparatus and performed measurement and analysis. R.C.A. supervised the work and performed analysis. O.E.D. and R.C.A. prepared the manuscript. L.N.P. and

K.W.W. performed the crystal growth. This work was sponsored by the Basic Energy Sciences Program of the Office of Science of the US Department of Energy, contract number FG02-08ER46514.

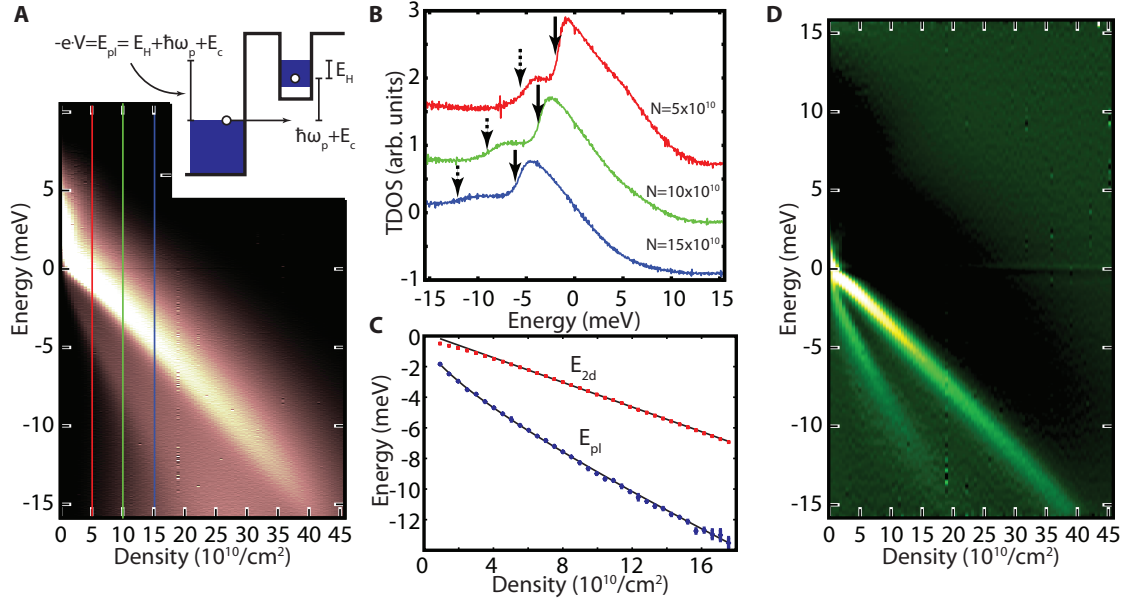


Figure 1: TDCS spectra acquired at zero magnetic field display both a 2D band edge, and a second “plasmaron” edge at lower energies. In **A**, the 2D band edge appears as a sharp peak due to tunneling matrix element effects. The plasmaron is visible as a faint second step at more negative energies. A small cartoon shows the measured energy of the plasmaron is negative, and roughly equal to the sum of the energy of the required hole, the required plasmon, and a coupling energy. The two edges are indicated in the linecuts in **B** (offset vertically for clarity), with the band edge indicated with a solid arrow, and the plasmaron edge indicated with a dotted arrow. In **D**, the band edges can be emphasized by taking an extra derivative of the data along the energy axis ( $d^2I/dV^2$ ). Defining the “edge” as the peak in  $d^2I/dV^2$ , this allows the energies of the 2D band edge (red) and plasmaron band edge (blue) to be extracted, as shown in **C**. Note the extreme asymmetry of the plasmaron band about the Fermi energy, ruling out inelastic scattering as a possible origin.

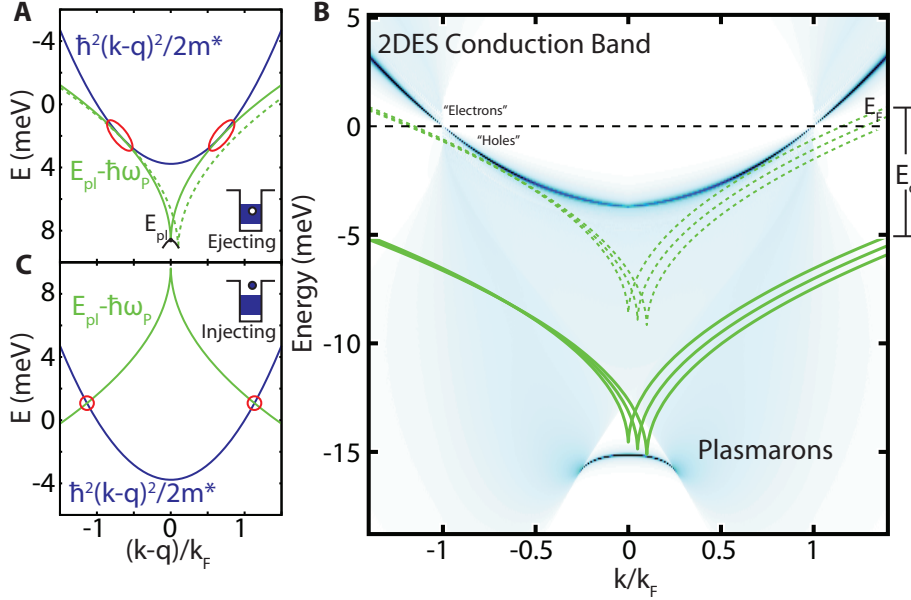


Figure 2: A simple cartoon model for the plasmaron can be developed by considering the resonance condition for the dispersion curves. In A, the tangency between the hole (blue) and plasmon (green) dispersion results in a large phase-space enhancement for hole-plasmon coupling (red circles), resulting in the long-lived plasmaron (black line). The  $y$ -axis has been drawn with more energetic holes downward to match the sign convention in our spectrum. A more accurate RPA calculation of the spectral function  $A(k, \omega)$ , roughly the momentum resolved SPDOS, is shown as a colorscale plot in (B). Dark blue peaks corresponding to the normal electron/hole and the plasmaron are visible. The general behaviour is consistent with the “cartoon” model (solid blue, green lines) if a fixed coupling energy  $E_C$  of about 5 meV is included (dashed green lines). If this argument is repeated for electrons (C), the dispersions cross at a sharp angle rather than tangentially, and there is no phase-space enhancement. In C, more energetic electrons are plotted upwards to match the sign convention in our spectrum.

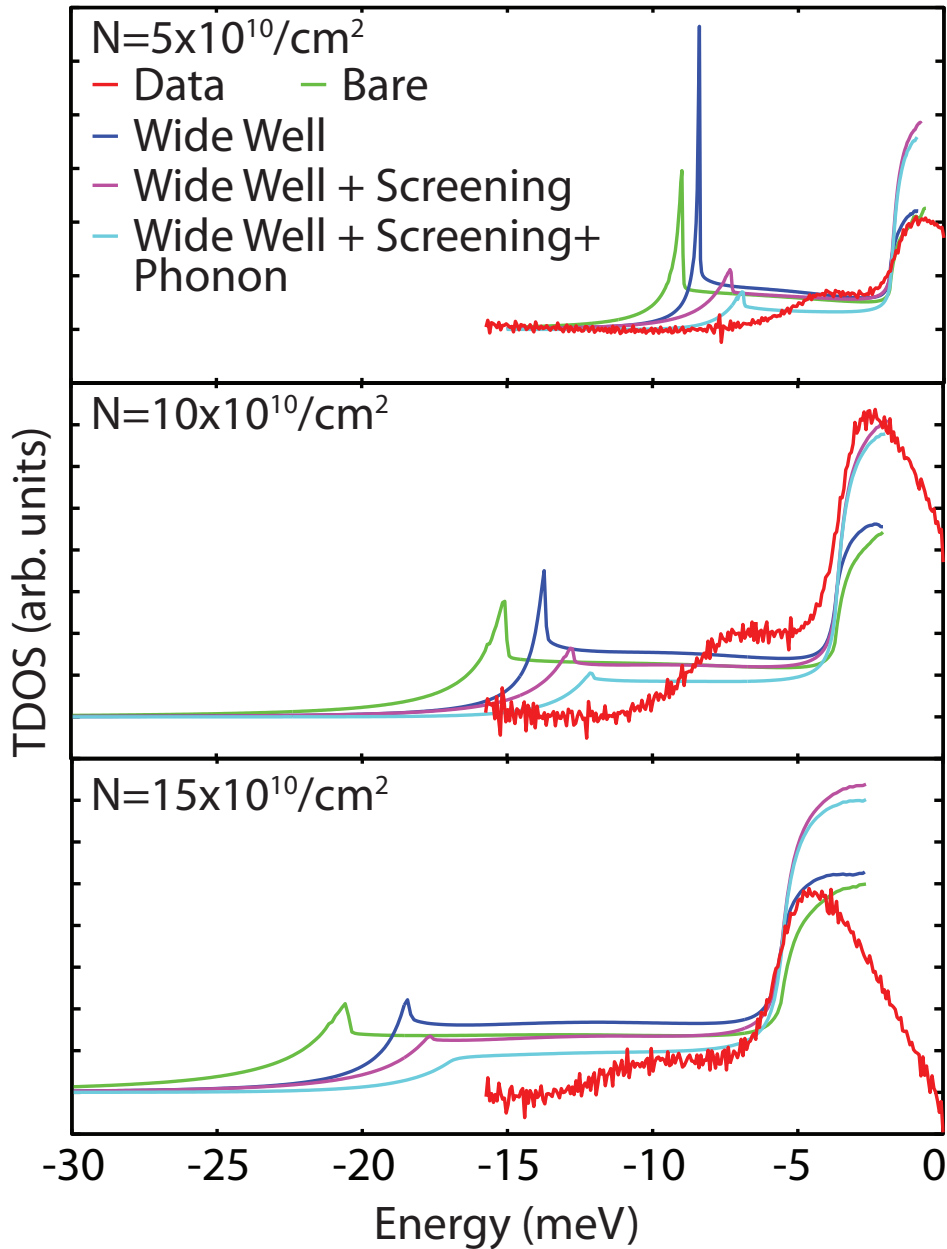


Figure 3: Comparison of measured TDCS spectra to RPA calculations. Up to an arbitrary scale factor in the TDOS axis and smooth distortions due to matrix element effects, the measured spectra can be quantitatively compared to theoretical calculations. Here, comparisons are made to a calculation with the bare Coloumb potential (Bare), a calculation in a  $230\text{\AA}$  square quantum well (Wide Well), a calculation in a  $230\text{\AA}$  well including screening from a nearby metallic electrode (Wide Well + Screening), and a calculation that also includes phonon coupling (Wide Well + Screening + Phonon). All of these overestimate the coupling energy of the plasmaron and the size of the peak at the plasmaron edge, but as the Coloumb interaction is softened, the agreement between the calculation and the experiment grows better.

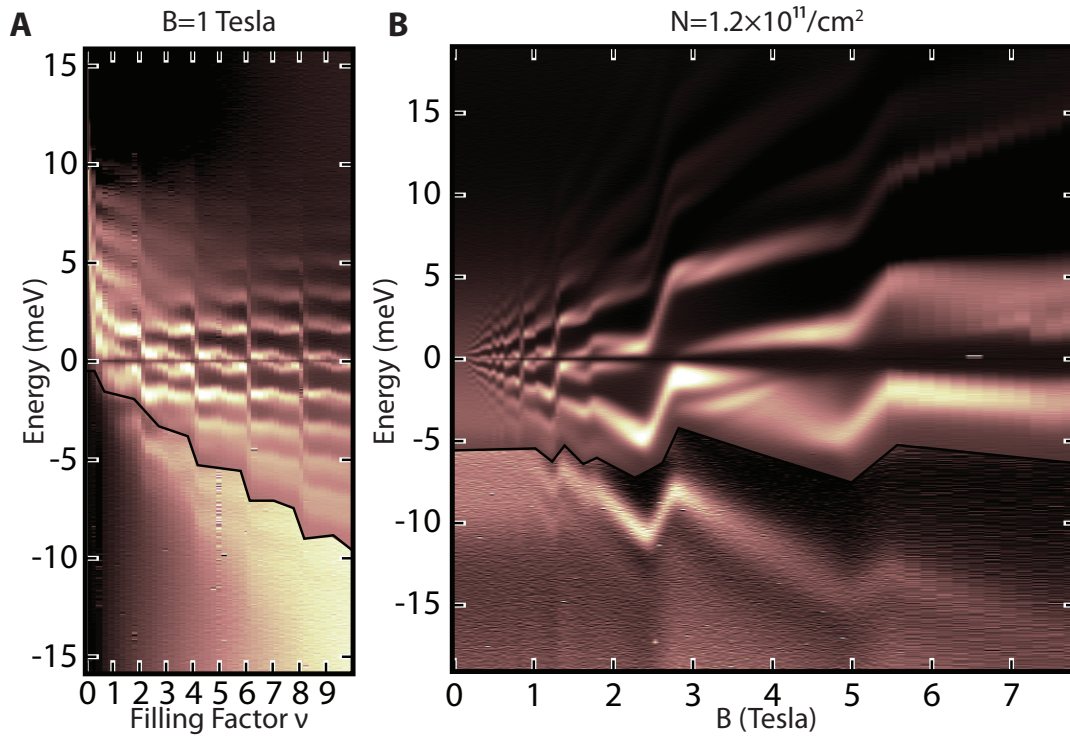


Figure 4: TDCS spectra showing the development of a magnetoplasmaron. Sweeping density at a fixed field of 1 Tesla (A), the “magnetoplasmaron” appears as a series of “ghost” Landau levels  $\hbar\omega_c$  below the  $N = 0$  Landau level. On holding the density fixed and sweeping the magnetic field, the separation between the “magnetoplasmaron” and the  $N = 0$  Landau level is seen to vary linearly with  $B$  as  $\hbar\omega_c$ , and can be seen to merge into the  $B = 0$  plasmaron band. The contrast has been enhanced below the black line just below the 2D band edge to show the plasmaron feature more clearly.